Basal melt rates beneath Whillans Ice Stream, West Antarctica

Lucas H. BEEM,[1,*] Ken C. JEZEK,[1] C.J. VAN DER VEEN[2]

[1]*Byrd Polar Research Center, The Ohio State University, 1090 Carmack Road, Columbus, Ohio 43210-1002, USA*
E-mail: lhbeem@gmail.com
[2]*Center for Remote Sensing of Ice Sheets and Department of Geography, University of Kansas, 213 Lindley Hall, 1475 Jayhawk Blvd, Lawrence, Kansas 66045-7594, USA*

ABSTRACT. Basal water lubricates and enables the fast flow of the West Antarctic ice streams which exist under low gravitational driving stress. Identification of sources and rates of basal meltwater production can provide insight into the dynamics of ice streams and the subglacial hydrology, which remain insufficiently described by glaciological theory. Combining measurements and analytic modeling, we identify two regions where basal meltwater is produced beneath Whillans Ice Stream, West Antarctica. Downstream of the onset of shear crevasses, strong basal melt (20–50 mm a^{-1}) is concentrated beneath the relatively narrow shear margins. Farther upstream, melt rates are consistently 3–7 mm a^{-1} across the width of the ice stream. We show that the transition in melt-rate patterns is coincident with the onset of shear margin crevassing and streaming flow and related to the development of significant lateral shear resistance, which reorganizes the resistive stress regime and induces a concentration of basal resistance adjacent to the shear margin. Finally, we discuss how downstream freeze-on in the ice-stream center coupled with melt beneath the shear margin might result in a slowing but widening ice stream.

INTRODUCTION

Basal melt represents the main source of subglacial water in West Antarctica. Mapping the spatial patterns and rates of basal melt contributes to understanding ice-sheet dynamics, sliding parameterization and subglacial hydrology, including subglacial lakes. Meltwater production, transport, refreeze and discharge constrain the speed of West Antarctic ice streams that are fast-moving conduits responsible for transporting most of the ice accumulated in the interior ice sheet and into the Ross Ice Shelf (Price and Whillans, 1998). For example, Whillans Ice Stream (WIS) flows at high speeds reaching ~700 m a^{-1} with driving stresses less than 20 kPa. This condition is enabled by lubricating basal water which weakens subglacial sediments, resulting in lowered basal resistance. Changes in the volume and pressure of the basal meltwater reservoir, including the draining or filling of subglacial lakes situated beneath the Siple Coast ice streams (Fricker and others, 2007; Smith and others, 2009), along with changes in longitudinal stress gradients due to changes in terminal geometry (i.e. grounding line position, ice shelves) are the two time-varying boundary conditions which can allow for rapid change of ice-stream dynamics (Retzlaff and Bentley, 1993; Stearns and others, 2005; Vaughan and Arthern, 2007).

Determining where meltwater is produced is a natural starting point for any study of the subglacial hydrology. Previous assessments of basal melt production below the Siple Coast ice streams (Parizek and others, 2003; Joughin and others, 2004) concluded that basal melt occurs primarily in the tributary regions where high driving stress (>20 kPa) is mostly compensated by basal drag. Localized areas of elevated melt are present throughout the ice stream and may be related to 'sticky spots', areas of elevated basal drag. Basal freeze-on is predicted in the interior of the main trunk of the ice stream and on the ice plain adjacent to the Ross Ice Shelf.

In this paper, we identify regions of basal meltwater production below WIS and its major tributaries, through the use of an analytical model that describes transverse variations in basal melting caused by frictional heating from basal drag below the interstream ridge, the shear margin and the ice stream. We find that basal melting is largely confined to a zone beneath the shear margins for the downstream segments of the ice stream. We go on to suggest how melting beneath the shear margin can lead to ice-stream widening.

THEORY

Whillans and Van der Veen (2001) proposed a model for estimating basal drag under the interstream ridge and across the ice stream. Essentially, the model describes the transformation of shearing over planes parallel to the bed (basal drag) and beneath the slow-moving interstream ridge into shearing along planes parallel to the ice-stream shear margin (lateral drag). The basic idea is that resistance arising from basal drag below the interstream ridge rotates into lateral forces that resist flow of the interior ice stream over its nearly frictionless base. Establishing the form of that stress transmission and depth variation of lateral stress yields an estimate of basal drag variations across the ice-stream margin.

The gravitational forces within the ice stream are largely balanced by the lateral drag developed along the margins (Jackson and Kamb, 1997; Whillans and Van der Veen, 1997; Harrison and others, 1998; Van der Veen and others, 2007). Absence of important longitudinal stress gradients allows for a simplification of the force-balance equations and the development of an analytical equation for basal drag. The approach is detailed by Whillans and Van der Veen (2001, equations (7–14)) who begin with a depth

*Present address: University of California, Santa Cruz, 1156 High Street, Santa Cruz, California 95064-1077, USA.

integration of the flow law linking shear strain rate acting between horizontal planes to shear stress. To obtain an analytic solution that relates basal drag to measured surface speed, they introduce a vertically varying weighting function on the basal drag. The approach is similar to that of Echelmeyer and others (1994) who show that as long as longitudinal stress gradients are small, horizontal drag varies linearly with depth. We expand the concept by empirically accommodating additional conditions (e.g. depth-varying hardness) by allowing the weighting to be exponential, with the exponent m to be either 1, 2 or 3.

Integrating vertical shear over the ice thickness yields

$$U(h) - U(b) = \int_b^h 2\frac{{R_e}^{n-1}R_{xz}}{B^n}\,\mathrm{d}z. \quad (1)$$

Here $U(h)$ and $U(b)$ are ice velocities at the surface and bed, respectively, n is the flow-law exponent, R_{xz} is vertical shear stress, B is the rate factor and R_e is the effective shear stress, defined as

$$R_e = \left({R_{xz}}^2 + {R_{xy}}^2\right)^{1/2}. \quad (2)$$

Introducing a depth-varying weighting function,

$$\left(\frac{{R_e}^{n-1}}{B^n}R_{xz}\right)^{1/n} = \left(\frac{h-z}{H}\right)^m \frac{\tau_b}{B_b}, \quad (3)$$

leads to (Whillans and Van der Veen, 2001, equation (14))

$$\tau_b = B_b\left(\frac{mn+1}{2H}U(h)(1-S)\right)^{1/n}. \quad (4)$$

Here τ_b is the basal drag in the along-flow direction, B_b is the rate factor appropriate for the warmer basal ice, H is ice thickness, and $S = U(b)/U(h)$ is the sliding ratio which varies laterally across the shear margin. Basal drag, τ_b, basal velocity, $U(b)$, basal temperature gradient, $\partial T/\partial z(b)$, estimates of geothermal flux, G, plus knowledge of basal ice properties, density, ρ, latent heat of fusion of ice, L_i, and thermal conductivity, k, are used to compute the amount of melt beneath the ice stream. S, U, H and τ_b each vary across the flow direction.

By assuming basal ice is at the pressure-melting point and that there is no horizontal heat advection, melt rates, M, are calculated from

$$\dot{M} = \frac{1}{\rho L_i}\left(G - k\frac{\partial T}{\partial z}(b) + \tau_b U(b)\right). \quad (5)$$

Note that the mathematical formulation leading to Equation (4) resembles the analytical model discussed by Echelmeyer and others (1994) and later adopted by Scambos and others (1994) to interpret velocity gradients across Ice Stream D (Bindschadler Ice Stream; compare Echelmeyer and others, 1994, equation (9) with equation (12) of Van der Veen and others, 2007). The important physical difference is that in the Echelmeyer model, velocities across the shear margin are modeled using an enhancement factor, E, on the lateral shearing as might occur if the ice in the margin is softened through crystal alignment. In our model, velocities across the margin are modeled by invoking a second constraint that links basal drag to the measured surface speed through the sliding fraction, ultimately resulting in the melting predicted by Equation (5). While both models contain an unknown and adjustable parameter, the shape and magnitude of S is better constrained as this function must increase monotonically from zero under the ridge to close to unity under the ice stream. The enhancement factor, on the other hand, is essentially unconstrained, both in how it varies laterally and in magnitude.

Each of the variables, except the sliding ratio, in Equations (4) and (5) is measured or calculated from the available datasets. The sliding ratio must be close to zero (no sliding) on the interstream ridge. Observations of basal pore-water pressure on the interior ice stream show the water pressure is nearly equal to the ice overburden (Kamb, 2001), and analysis of tills beneath the ice stream shows a yield strength of only a few kPa (Tulaczyk and others, 2000). This supports the assumption that the sliding ratio must approach unity within the ice stream.

The transition from no sliding to full sliding is estimated using an approach outlined by Van der Veen and others (2007). The basic idea is that forces from basal drag on the interstream ridges must balance both the force associated with the local driving stress of the slow-moving ridge ice and the shearing forces that restrain the entire ice stream (Whillans and Van der Veen, 1997). Excess basal drag, F, at a point is the fraction of the total drag that contributes to supporting the ice stream across the shear margin. It is given as the integral of the difference between the basal drag, τ_b, and the driving stress, τ_d, along a line from the interstream ridge to a point within the ice stream:

$$F(y) = \int_0^y \left[\tau_b(y) - \tau_d(y)\right]\mathrm{d}y. \quad (6)$$

The position of complete sliding is located where excess basal drag generated outside the ice stream is equal to the amount of lateral drag offered by the shear margin. The magnitude of lateral drag offered by the shear margin can be estimated as the product of ice thickness and the maximum lateral shear stress within the margin (Van der Veen, 1999, p. 125):

$$F_{lat} = B\left(\frac{\dot{\epsilon}_{xy}}{2}\right)^{1/n}H. \quad (7)$$

In this equation the strain rate, $\dot{\epsilon}_{xy}$, is taken as the maximum value within the shear margin and B as a depth-averaged value of the rate factor.

We select a point to begin integrating excess basal drag by noting that basal drag below the interstream ridge far from the shear margin is expected to be nearly equal to the local driving stress and therefore should have little effect on the form of the integrated excess basal drag curve. We begin integration of excess basal resistance at the location where lateral strain rates consistently exceed values found at the center of the interstream ridge. Next, when the integration of excess basal drag working from the interstream ridge toward the ice stream equals the magnitude of the lateral resistance offered by the shear margin, we set the sliding ratio equal to unity (see Fig. 1b and c).

This method determines the most marginward location of complete sliding but not the location where sliding begins. We prescribe a surface velocity threshold of 30 m a^{-1} above which there is a component of sliding (see Fig. 1c and d). The actual velocity where sliding begins is not known and is likely to vary due to stress heterogeneity and flow history. Within the interstream ridge, where the base is frozen to the bed and sliding zero, velocities approach 10 m a^{-1}. A simple laminar flow model underestimates the amount of internal deformation. Using a rate factor appropriate for –5°C, $H = 1000$ and $\tau_b = 20$ kPa, the model predicts <20 cm a^{-1} of surface velocity from ice deformation. 30 m a^{-1} of internal

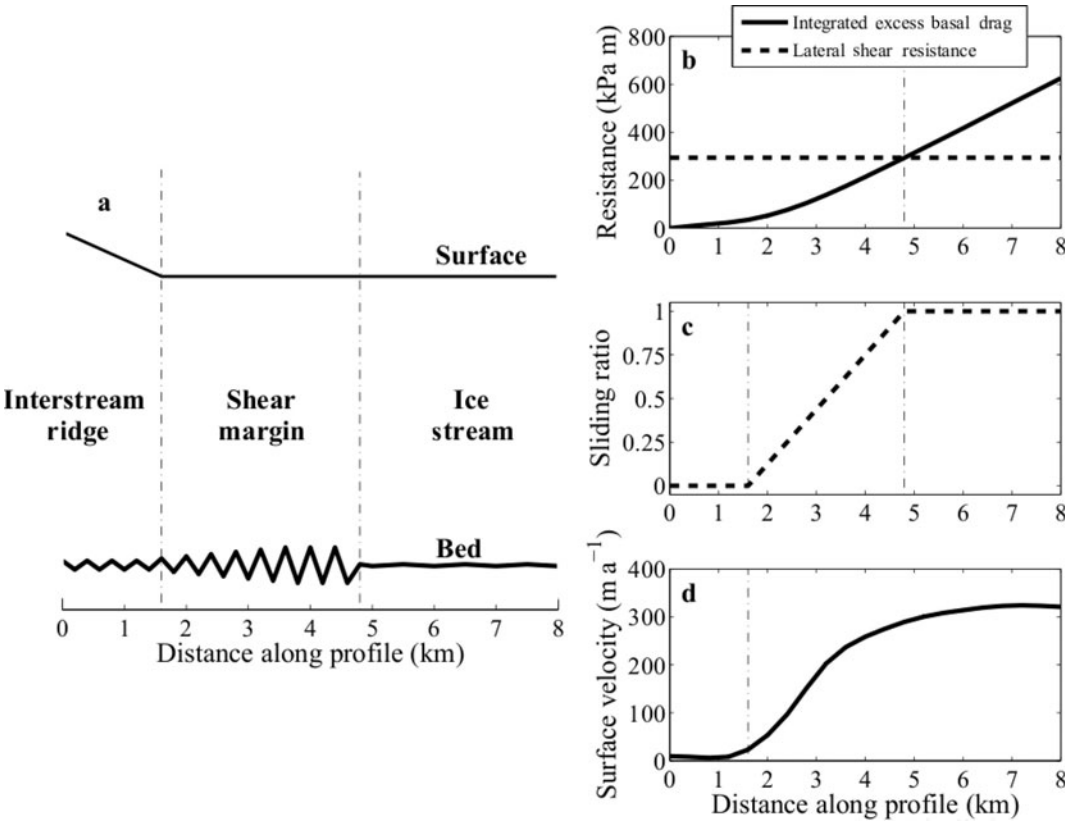

Fig. 1. Schematic geometry of sliding ratio parameterization, where (a) basal topography represents relative basal drag magnitude for an idealized profile. Integration of excess basal resistance (b; Equation (6)) determines the point where it exceeds lateral strain rate (Equation (7)). At this point (c), the sliding ratio is set to 1. Maximum lateral resistance is plotted to illustrate the threshold and not as a spatially dependent variable. The surface velocity with threshold of 30 m a^{-1} is shown in (d) at the location there the sliding ratio first exceeds zero. Note consistent horizontal scale for each panel, and vertical line between panels to illustrate interstream ridge, shear margin and interior ice stream.

deformation using a laminar flow model requires a temperature of 0°C and a driving stress of 55 kPa, or inclusion of an enhancement factor of approximately 5 which is well within the range of published studies (Echelmeyer and others, 1994). In the ice-stream margins, flow enhancement from strain fabric and viscous dissipation is expected. Each of these conditions will raise the amount of internal deformation possible. As a result, 30 m a^{-1} represents a reasonable estimate for a velocity threshold in which there is a component of basal sliding. Furthermore, due to basal melt-rate dependence on the sliding velocity (Equations (4) and (5)) and surface velocity less than 30 m a^{-1}, moving the location of initial sliding marginward has a minor impact on the amount of basal heat generated.

The velocity threshold also roughly coincides with the most marginward location of shear crevassing. Although it is not supposed that basal processes translate to the surface in such a simple manner, it offers some physical constraints on the location of initial sliding. The sliding ratio is assumed to vary linearly from $S = 0$ at this point to $S = 1$ at the position determined through the integration of excess basal drag. Other functional relations could be adopted for transverse variations in sliding ratio, but this has little impact on the results obtained here.

Although lateral resistance primarily supports the driving stress of the ice stream, total resistance, the integration of the driving stress across the ice stream, exceeds lateral resistance. To achieve force balance, there must be residual basal drag within the ice stream, contrary to our assumption that the sliding ratio is exactly equal to unity. For WIS this usually amounts to basal drag of 1–2 kPa. However, the dependence of basal drag on surface velocity (Equation (4)) means that the sliding ratio need only be within a few percent of unity to yield the required 1–2 kPa of basal drag.

DATASETS

We use four primary datasets to estimate basal melt over the length of the ice stream: the British Antarctic Survey's BEDMAP (Lythe and others, 2001) for ice thickness; the OSU DEM (Ohio State University Digital Elevation Model) relative to the geoid (Liu and others, 1999) for ice surface slope; the RADARSAT-1 Antarctic Mapping Project (RAMP) mosaic (Jezek, 1999) for ice-stream dimensions; and interferometric synthetic aperture radar (InSAR) surface velocities from RADARSAT-1 (Joughin and others, 1999). Other sources of published data used include temperature measurements from boreholes (Kamb, 2001; Engelhardt, 2004a) and estimates of geothermal flux (Rose, 1979; Alley and Bentley, 1988; Engelhardt, 2004a).

MODEL SENSITIVITY

Spatially uniform parameter values were chosen for the basal melt calculation. Although some model parameters are expected to vary spatially, the paucity of observations

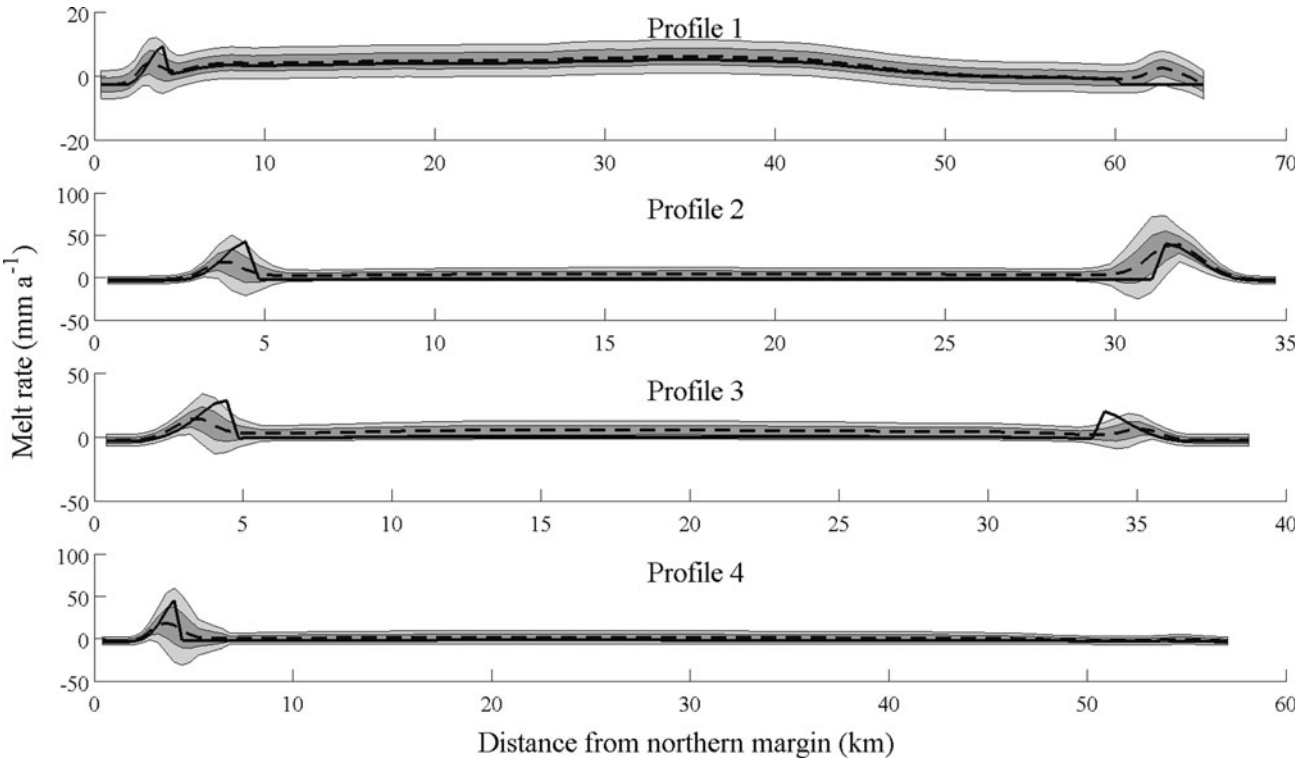

Fig. 2. Sensitivity of model to assumed parameter uncertainty over different profiles. Average of 300 iterations (dashed black curve) with standard deviation ($\pm 1\sigma$ dark gray region and $\pm 2\sigma$ light gray region) is plotted against the results shown in Figure 3 (solid black curve). See Figure 3 for profile locations.

makes that determination tenuous. To investigate the sensitivity of our model, we assigned a range of possible values to variables used in the melt-rate calculation. Each variable was assumed to have a Gaussian distribution centered on the expected or measured value. Measured variables were assigned a $\pm 2\sigma$ standard deviation based on published error estimates, while constants were prescribed an expected range. The following variables and their associated standard deviations are used in the analysis: surface velocity (measured $\pm 12\,\mathrm{m\,a^{-1}}$); ice thickness (measured $\pm 60\,\mathrm{m}$ as reported by Retzlaff and others (1993)); driving stress (measured $\pm 4\,\mathrm{kPa}$); basal rate factor ($120 \pm 40\ \mathrm{kPa\,a^{-1/3}}$); depth-averaged rate factor ($500 \pm 40\,\mathrm{kPa\,a^{-1/3}}$); basal ice density ($917 \pm 8\,\mathrm{kg\,m^{-3}}$); geothermal flux ($60 \pm 10\,\mathrm{mW\,m^{-2}}$); thermal conductivity ($2.1 \pm 0.005\,\mathrm{W\,(m\,^{\circ}C)^{-1}}$); and basal temperature gradient ($0.04 \pm 0.02\,^{\circ}\mathrm{C\,m^{-1}}$). A value for each of these variables was randomly chosen given its probability distribution, and a solution of melt rate was generated. To generate probability distributions for basal melt rate, this procedure was repeated 300 times, 100 each with $m = 1$, 2 or 3. Four profiles (Fig. 2), chosen to represent various patterns of melt-rate distribution found beneath the ice stream, show a consistent picture of elevated melt below the shear margin albeit with variability in the magnitude of the melt peak. Even with the uncertainty in melt-rate magnitude, 50–100% of the melt volume originates from a narrow band below or adjacent to the margin of the ice stream. For the interior ice of the stream, and where there is little melt concentration below the shear margin, the uncertainties become sufficient to mask whether freezing or thawing occurs at the base.

The assumption of simple shear limits the upstream extent of the calculations. Above the commencement of shear crevassing of WIS, the amount of transverse flow increases appreciably. This increases the importance of normal resistive stresses and compromises the heuristic form of depth variation in R_{xz}. Furthermore, the assumption that the basal topography is nearly flat begins to break down above the location of the shear crevassing onset (Retzlaff and others, 1993) and may not be valid for the entirety of Mercer Ice Stream.

Our model does not explicitly incorporate the effects of strain heating. This is treated by selecting an appropriate depth-averaged rate factor. If the rate factor is too high, strain heating that is not accounted for could affect our results by decreasing the basal thermal gradient or lowering the magnitude of lateral resistance offered by the margin. Decreased basal thermal gradient will increase calculated basal melt rates by limiting vertical heat conduction into the ice. The sensitivity analysis shows a possible increase in melt rate of $\sim 6.6\,\mathrm{mm\,a^{-1}}$ if $\partial T/\partial z < 0.01\,\mathrm{m\,^{\circ}C^{-1}}$. The areas with maximum viscous heating are also the areas with elevated basal drag. This represents a maximum increase of 10–20% of the total basal melt predicted.

More significantly, enhancement due to favorably aligned fabric in the shear margin or thermal softening of ice in the shear margin would lower the amount of lateral resistance here. This would lower the amount of excess basal resistance required to generate lateral shearing, decreasing the basal drag concentration, and will lead to lower basal melt beneath the shear margin. We believe that a depth-averaged rate factor appropriate for ice of $-15^{\circ}\mathrm{C}$ accounts for a significant amount of strain fabric or thermal softening in the shear margin. Supporting this, our chosen rate factor yields a lateral resistance which nearly supports the entirety of driving stress, consistent with previous studies, and results in

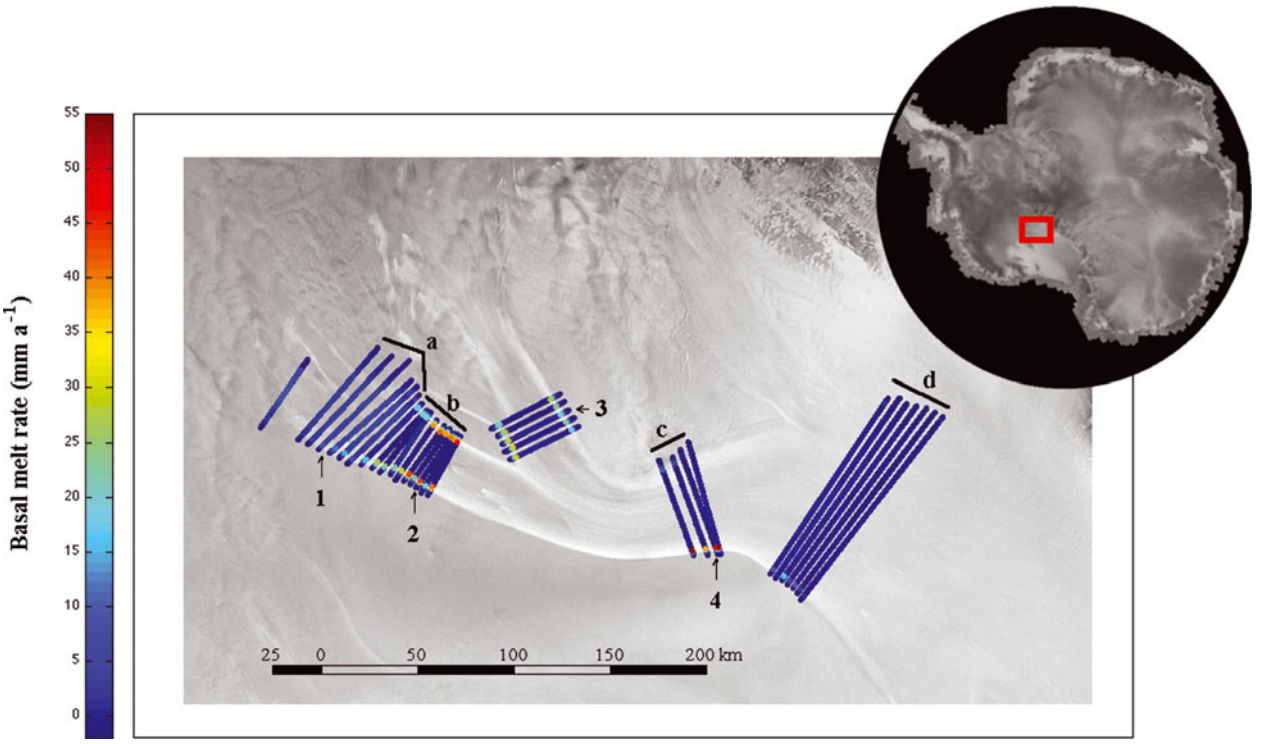

Fig. 3. Model results for basal melt rates (mm a^{-1}) overlaid on the RAMP mosaic. Example profiles used in sensitivity analysis (Fig. 2) are marked as 1–4 and regions where melt volumes are calculated in the text are labeled a–d.

interior basal drag consistent with measured yield strengths of subglacial till (Tulaczyk and others, 2000).

RESULTS

Thirty-three transverse profiles were used to estimate the spatial variability of the basal melt rates below WIS and Van der Veen Ice Stream (Fig. 3). Two melt-rate patterns are identifiable in the results. One is where a high melt rate, 20–50 mm a^{-1}, is concentrated beneath a narrow region beneath or adjacent to the shear margin and with little to no melt or even freeze-on conditions across the interior of the ice stream (e.g. profile 2 in Fig. 3). The other pattern is one where melt at intermediate levels, 3–7 mm a^{-1}, is distributed across the entire width of the ice stream and there is minimal or nonexistent melt beneath the shear margin (e.g. profile 1 in Fig. 3). These will be referred to respectively as concentrated and distributed patterns of melt.

Concentrated melt characterizes most of WIS. Progressing upstream from near the grounding line, every profile shows concentrated melt below the shear margin. However, upstream of the start of shear crevassing, located near profile 1 of Figure 3 for the northern margin, and further downstream by four profiles for the southern margin, the profiles show a distributed melt pattern. This is mainly caused by diminished lateral resistance and increased driving stress. These conditions limit concentration of basal drag near the shear margins and require bed resistance to be more widely distributed across the entire width to achieve force balance. Many of the melt-rate profiles show asymmetry because of different shear stresses and ice thicknesses between the two sides of the ice stream.

Bindschadler and others (2001) define streaming-flow onset as the transition from flow largely balanced by basal drag to flow where basal drag is largely absent. The transition from a distributed to a concentrated melt pattern is roughly the location of the appearance of shear margin crevassing and the location where basal drag across the interior diminishes appreciably. This can be seen in Figure 4a, as basal melt switches to freezing and melt rates beneath the shear margin (Fig. 4b) correspondingly increase. The location where interior basal melt transitions to freeze-on conditions is exactly the region where shear margin crevassing initiates. There is clearly a relationship between the onset of shear crevasses, onset of full streaming flow and transition from one melt pattern to the other.

Presumably, distributed melt upstream creates an areally extensive layer of basal water capable of influencing basal conditions over the entire width of the ice stream. Once the basal water layer becomes thick enough, or pressurized enough, basal resistance is no longer able to fully balance driving stress. This eventually leads to shear margin crevassing and the concentration of basal melt beneath the shear margins. This transition occurs over an approximately 30 km long section of the ice stream.

Once full streaming flow commences on WIS, minimal melt is generated beneath the interior of the ice stream. Due to the large surface area of the interior of the ice stream, where $S \approx 1$, the uncertainty in melt rate leads to great uncertainty in total melt volume. However, using our best-guess parameters and the mean from the sensitivity tests, we suggest that there is an upstream region of net melt production transitioning to net freeze-on conditions in the downstream regions. The farthest upstream region (a in Fig. 3) exhibits a distributed melt pattern and produces nearly 6.5×10^6 m^3 a^{-1} of water (1.4 mm a^{-1} m^{-2}). The next downstream region and the first with a concentrated pattern (b in Fig. 3) produces meltwater at a rate of 2.0×10^6 m^3 a^{-1} (0.5 mm a^{-1} m^{-2}). Farther downstream, melt gives way to net freeze-on conditions of -1.0×10^6 m^3 a^{-1} (–0.5 mm a^{-1} m^{-2})

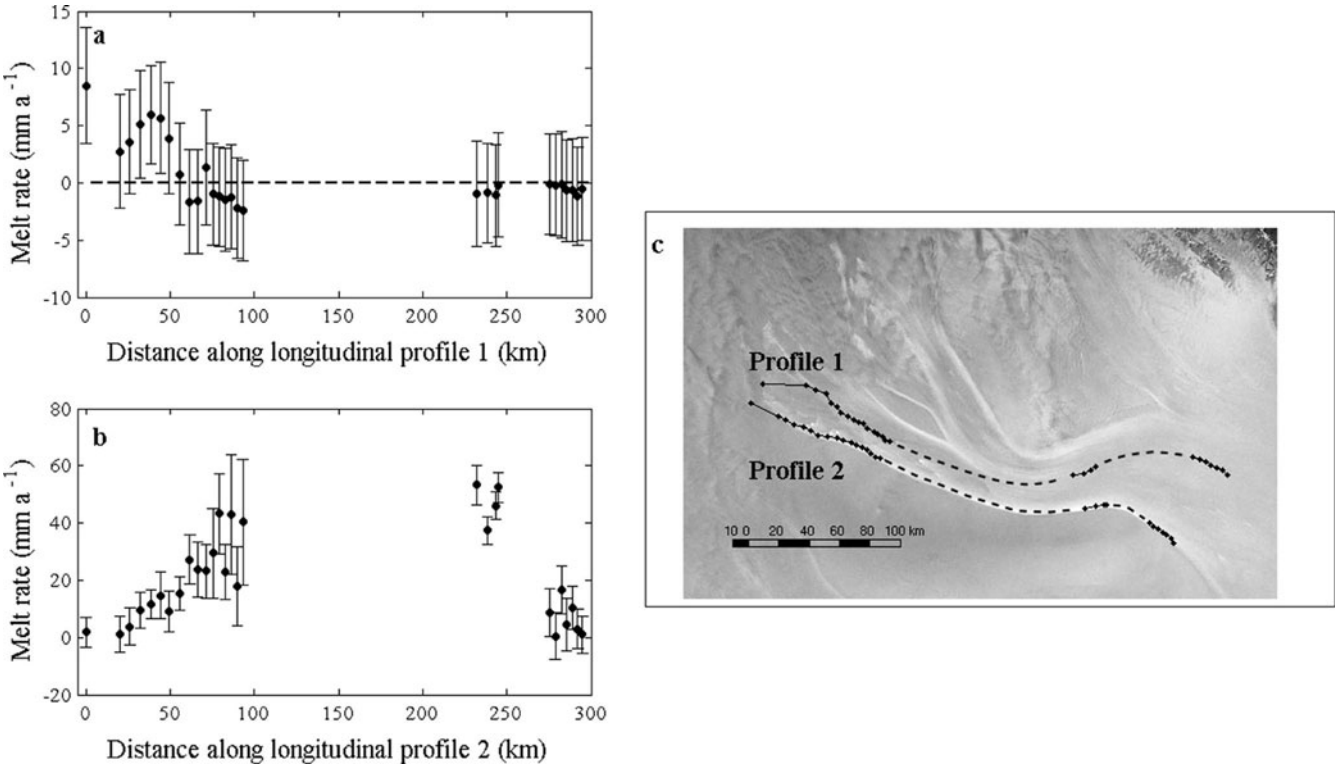

Fig. 4. Longitudinal variations in the basal melt rate along two profiles (a, b) beginning at the upstream limit, with profile locations shown in (c). The dashed portions of the profiles are areas without data. Error bars are $\pm 2\sigma$ taken from the standard deviation of the sensitivity analysis (see example profiles in Fig. 2). Melt rate along the interior of the ice stream (a; profile 1) shows the transition from distributed melt to concentrated melt, when interior melt approaches 0 mm a^{-1} or freeze-on conditions. This transition coincides with increases in the maximum melt-rate peak below the shear margin (b; profile 2). Downstream variations in peak melt rate result from a combination of variable lateral resistance and decreasing driving stress.

of water (region c in Fig. 3), and -3.5×10^6 m^3 a^{-1} (-0.8 mm a^{-1} m^{-2}) of water (region d). Note that these estimates do not include any melt generated in the catchment of WIS, upstream of profiles. In total, the volume of water generated above the full streaming-flow onset could be enough to lubricate the remainder of the ice stream (Parizek and others, 2002).

WIS has been slowing and widening over time (Joughin and Tulaczyk, 2002; Stearns and others, 2005). Based on the conclusion that lateral drag supports most of the driving stress, Van der Veen (1999, p. 168) proposed a model linking center-line velocity to the fourth power of ice-stream width. This creates the condition that a wider ice stream is also a faster one provided the driving stress remains the same.

Jacobson and Raymond (1998) showed that in order for the ice stream to be thermally widened, thermal conduction must overcome advection of colder interstream ice into the ice stream. Their models showed that transverse velocities of 2 m a^{-1}, consistent with measurements on WIS, would be enough to limit ice-stream widening. However, their model does not include the excess heat generated at the base through elevated basal drag predicted by our model. They stated that if geothermal flux is large enough, it would be possible to widen the ice stream with transverse velocities as great as 10 m a^{-1} into the ice stream. Our excess heat generation can be treated as localized elevated heat flux and could serve to buffer against cold-ice advection.

Any heat that is used to warm basal ice beneath the interstream ridge or ice advected into the ice stream will not be available for melt and will lower our estimates accordingly. However, the amount of energy needed to warm basal ice of 50 m thickness by 3°C, with a transverse velocity of 10 m a^{-1}, is approximately 3×10^9 J m^{-1} of ice-stream length. Integration of basal friction across the shear margin yields the amount of energy per unit length of the ice stream. These values range from 0.4×10^9 to 25×10^9 J m^{-1} depending on the amount of concentrated basal resistance determined by the model. In high shear strain regions, viscous dissipation will also serve to warm interstream ice as it enters the ice stream. There is ample energy in our model to thaw cold basal ice and still produce high basal melt rates. The regions of highest basal melt rates, along the northern margin of the ice stream, correspond to the regions of greatest shear margin migration reported by Stearns and others (2005).

The mechanism governing redistribution of basal water will also control advection of heat. The inferred presence of a hydrologic pressure ridge that runs parallel to the shear margin (Fricker and others, 2007) may act to further concentrate heat by keeping basal water proximal. Furthermore, the borehole investigations of Engelhardt (2004b) discovered under-pressured channelized water downstream of areas of high melt production beneath Kamb Ice Stream. Also, basal-water routing models (Le Brocq and others, 2009) suggest a concentration of basal water along the northern margin of WIS.

It is reasonable to expect that the slowdown of WIS is related to a reorganization of the basal hydrology system into a lower-pressure channelized system. Although this is beyond the scope of this work, it suggests that basal water may remain in a relatively narrow longitudinal band minimizing advection of heat and not serving to lubricate the interior ice stream.

The findings presented here offer a new hypothesis for controls on changes in ice-stream flow and, in particular, the observed slowing and widening of WIS. Once lateral resistance supports most of the driving stress, basal drag across the interior is small (<2 kPa). Despite basal velocities of 500–700 m a^{-1}, the dynamic friction is insufficient to melt basal ice as it may not be able to generate enough heat to compensate for conduction into the glacier, leading to basal freeze-on. Basal freeze-on, which strengthens subglacial sediments and physically attaches the base of the ice stream to the basal substrate, is one mechanism to explain center-line deceleration (Tulaczyk and others, 2000). Simultaneously, the margins adjacent to basal freeze-on regions are experiencing some of the highest local melt-rate magnitudes found anywhere in the ice-stream system. This excess heat could serve to thaw some of the interstream ridge and widen the area of basally lubricated flow.

Basal radar returns from over the northern shear margin of WIS show a curious lack of a transition between the interstream ridge and the interior ice stream (Raymond and others, 2006). Raymond and others (2006) suggest one explanation is that there is a thicker layer of particularly fresh water at these locations, which our model predicts.

CONCLUSIONS

The analytical model adopted here to estimate basal drag and melt rates provides a new perspective on understanding how basal drag, and thus melt rates, may be distributed across the ice stream. Basal drag across the width of the ice stream is important upstream of full streaming flow, supplying more than 40–50% of the total resistance to driving stress. This encourages the distributed pattern of basal melt and can produce large volumes of basal meltwater that, when further distributed downstream, reduces basal drag and increases the fraction of driving stress supported by lateral resistance. Our model strongly suggests the persistent occurrence of elevated melt rates concentrated beneath the shear margins once lateral stress nearly balances driving stress. The exact magnitudes of basal melt are subject to model uncertainty and local shear stress, but the patterns remain robust. These patterns offer a hypothesis to explain observed morphological changes of a slowing and widening ice stream by having center-line deceleration induced by basal freeze-on conditions adjacent to high melt rates concentrated at the margins. These results offer insights into the basal controls of the dynamics of ice streams, reinforcing the need to better understand the nature of basal hydrology on both spatial and temporal scales.

ACKNOWLEDGEMENTS

This research was supported by the US National Science Foundation (NSF) Center for Remote Sensing of Ice Sheets (NSF grant No. 0424589). We thank S. Anandakrishnan and an anonymous reviewer for their many helpful comments.

REFERENCES

Alley, R.B. and C.R. Bentley. 1988. Ice-core analysis on the Siple Coast of West Antarctica. *Ann. Glaciol.*, **11**, 1–7.

Bindschadler, R., J. Bamber and S. Anandakrishnan. 2001. Onset of streaming flow in the Siple Coast region, West Antarctica. *In* Alley, R.B. and R.A. Bindschadler, *eds. The West Antarctic ice sheet: behavior and environment*. Washington, DC, American Geophysical Union, 123–136. (Antarctic Research Series 77.)

Echelmeyer, K.A., W.D. Harrison, C. Larsen and J.E. Mitchell. 1994. The role of the margins in the dynamics of an active ice stream. *J. Glaciol.*, **40**(136), 527–538.

Engelhardt, H. 2004a. Ice temperature and high geothermal flux at Siple Dome, West Antarctica, from borehole measurements. *J. Glaciol.*, **50**(169), 251–256.

Engelhardt, H. 2004b. Thermal regime and dynamics of the West Antarctic ice sheet. *Ann. Glaciol.*, **39**, 85–92.

Fricker, H.A., T. Scambos, R. Bindschadler and L. Padman. 2007. An active subglacial water system in West Antarctica mapped from space. *Science*, **315**(5818), 1544–1548.

Harrison, W.D., K.A. Echelmeyer and C.F. Larsen. 1998. Measurement of temperature in a margin of Ice Stream B, Antarctica: implications for margin migration and lateral drag. *J. Glaciol.*, **44**(148), 615–624.

Jackson, M. and B. Kamb. 1997. The marginal shear stress of Ice Stream B, West Antarctica. *J. Glaciol.*, **43**(145), 415–426.

Jacobson, H.P. and C.F. Raymond. 1998. Thermal effects on the location of ice stream margins. *J. Geophys. Res.*, **103**(B6), 12,111–12,122.

Jezek, K.C. 1999. Glaciological properties of the Antarctic ice sheet from RADARSAT-1 synthetic aperture radar imagery. *Ann. Glaciol.*, **29**, 286–290.

Joughin, I. and S. Tulaczyk. 2002. Positive mass balance of the Ross ice streams, West Antarctica. *Science*, **295**(5554), 476–480.

Joughin, I. *and 7 others*. 1999. Tributaries of West Antarctic ice streams revealed by RADARSAT interferometry. *Science*, **286**(5438), 283–286.

Joughin, I., S. Tulaczyk, D. MacAyeal and H. Engelhardt. 2004. Melting and freezing beneath the Ross ice streams, Antarctica. *J. Glaciol.*, **50**(168), 96–108.

Kamb, B. 2001. Basal zone of the West Antarctic ice streams and its role in lubrication of their rapid motion. *In* Alley, R.B. and R.A. Bindschadler, *eds. The West Antarctic ice sheet: behavior and environment*. Washington, DC, American Geophysical Union, 157–199. (Antarctic Research Series 77.)

Le Brocq, A.M., A.J. Payne, M.J. Siegert and R.B. Alley. 2009. A subglacial water-flow model for West Antarctica. *J. Glaciol.*, **55**(193), 879–888.

Liu, H., K.C. Jezek and B. Li. 1999. Development of an Antarctic digital elevation model by integrating cartographic and remotely sensed data: a geographic information system based approach. *J. Geophys. Res.*, **104**(B10), 23,199–23,213.

Lythe, M.B., D.G. Vaughan and BEDMAP consortium. 2001. BEDMAP: a new ice thickness and subglacial topographic model of Antarctica. *J. Geophys. Res.*, **106**(B6), 11,335–11,351.

Parizek, B.R., R.B. Alley, S. Anandakrishnan and H. Conway. 2002. Sub-catchment melt and long-term stability of Ice Stream D, West Antarctica. *Geophys. Res. Lett.*, **29**(8), 551–554.

Parizek, B.R., R.B. Alley and C.L. Hulbe. 2003. Subglacial thermal balance permits ongoing grounding-line retreat along the Siple Coast of West Antarctica. *Ann. Glaciol.*, **36**, 251–256.

Price, S.F. and I.M. Whillans. 1998. Delineation of a catchment boundary using velocity and elevation measurements. *Ann. Glaciol.*, **27**, 140–144.

Raymond, C.F., G.A. Catania, N. Nereson and C.J. van der Veen. 2006. Bed radar reflectivity across the north margin of Whillans Ice Stream, West Antarctica, and implications for margin processes. *J. Glaciol.*, **52**(176), 3–10.

Retzlaff, R. and C.R. Bentley. 1993. Timing of stagnation of Ice Stream C, West Antarctica, from short-pulse radar studies of buried surface crevasses. *J. Glaciol.*, **39**(133), 553–561.

Retzlaff, R., N. Lord and C.R. Bentley. 1993. Airborne-radar studies: Ice Streams A, B and C, West Antarctica. *J. Glaciol.*, **39**(133), 495–506.

Rose, K.E. 1979. Characteristics of ice flow in Marie Byrd Land, Antarctica. *J. Glaciol.*, **24**(90), 63–75.

Scambos, T.A., K.A. Echelmeyer, M.A. Fahnestock and R.A. Bindschadler. 1994. Development of enhanced ice flow at the southern margin of Ice Stream D, Antarctica. *Ann. Glaciol.,* **20**, 313–318.

Smith, B.E., H.A. Fricker, I.R. Joughin and S. Tulaczyk. 2009. An inventory of active subglacial lakes in Antarctica detected by ICESat (2003–2008). *J. Glaciol.,* **55**(192), 573–595.

Stearns, L.A., K.C. Jezek and C.J. van der Veen. 2005. Decadal-scale variations in ice flow along Whillans Ice Stream and its tributaries, West Antarctica. *J. Glaciol.,* **51**(172), 147–157.

Tulaczyk, S.M., B. Kamb and H.F. Engelhardt. 2000. Basal mechanics of Ice Stream B, West Antarctica. I. Till mechanics. *J. Geophys. Res.,* **105**(B1), 463–481.

Van der Veen, C.J. 1999. *Fundamentals of glacier dynamics.* Rotterdam, A.A. Balkema.

Van der Veen, C.J., K.C. Jezek and L. Stearns. 2007. Shear measurements across the northern margin of Whillans Ice Stream. *J. Glaciol.,* **53**(180), 17–29.

Vaughan, D.G. and R. Arthern. 2007. Climate change: why is it hard to predict the future of ice sheets? *Science,* **315**(5818), 1503–1504.

Whillans, I.M. and C.J. van der Veen. 1997. The role of lateral drag in the dynamics of Ice Stream B, Antarctica. *J. Glaciol.,* **43**(144), 231–237.

Whillans, I.M. and C.J. van der Veen. 2001. Transmission of stress between an ice stream and interstream ridge. *J. Glaciol.,* **47**(158), 433–440.

MS received 7 January 2010 and accepted in revised form 23 June 2010